CHEMISTRY
A EUROPEAN JOURNAL

DOI: 10.1002/chem.200701473

Enolic Schiff Base Aluminum Complexes and Their Catalytic Stereoselective Polymerization of Racemic Lactide

Xuan Pang,[a, b] Hongzhi Du,[a, b] Xuesi Chen,*[a] Xianhong Wang,[a] and Xiabin Jing[a]

Abstract: A series of enolic Schiff base aluminum(III) complexes LAlR (where L = NNOO-tetradentate enolic Schiff base ligand) containing ligands that differ in their steric and electronic properties were synthesized. Their single crystals showed that these complexes are five-coordinated around the aluminum center. Their coordination geometries are between square pyramidal and trigonal bipyramidal. Their catalytic properties in the solution polymerization of racemic lactide (*rac*-LA) were examined. The modifications in the auxiliary ligand exhibited a dramatic influence on the catalytic performance. Lengthening the backbone from C_2 alkylene to C_3 alkylene resulted in remarkable enhancement of both the stereoselectivity and the polymerization rate because of the increasing flexibility of the diimine backbone. Electron-withdrawing substituents in the diketone also highly improved the activity and the stereoselectivity. Among these complexes, **4b** had the highest activity and the stereoselectivity owing to the C_3 alkylene backbone and the two *gem*-methyl groups on the middle carbon atom. The value of the polymerization rate constant (k_p) catalyzed by **4b** in 70 °C was 1.90 L mol^{-1} min^{-1}, the activation energy of the polymerization (35.4 kJ mol^{-1}) was calculated according to the Arrhenius equation. Other factors that influenced the polymerization, such as the polymerization time, the temperature, and the monomer concentration, are also discussed in detail.

Keywords: aluminum · lactide · ring-opening polymerization · Schiff bases · stereoselectivity

Introduction

Biodegradable polyesters have found a wide range of applications, such as sutures, bone fracture fixation devices, drug controlled release carriers, tissue engineering scaffolds and green plastics for wrapping materials, disposal containers and fibers.[1] Because the ester linkage is easily hydrolyzed, they can be converted into hydroxyl acid via degradation and finally to CO_2 and water. For these reasons, a lot of research on the biodegradable polyesters has been carried out in recent years.[2] Polylactide (PLA) is one of the most promising biodegradable polyesters because of its renewable resources.[3] PLA can be prepared by the ring-opening polymerization (ROP) of lactide (LA) or by direct condensation of lactic acid. Lactide exists as three different stereoisomers: L-lactide (L-LA), D-lactide (D-LA) and *meso*-lactide (Scheme 1), so their polymers may have different chain configurations (Scheme 2). The chain microstructures of PLA are one of the most important factors that influence the physical, mechanical and degradation properties of the polymers.[4] Conventional catalysts such as aluminum trialkoxides[5] and tin(II) octanoate[6] do not prefer one of the three different stereoisomers of LA, so the polymers obtained by these catalysts contain random placements of lactide monomers. The stereoregular polymers can be obtained contain by using either the enantiopure L-LA or D-LA monomer.

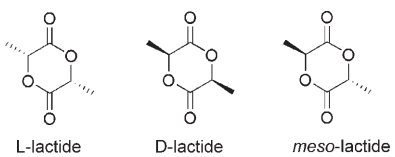

Scheme 1. Stereoisomers of lactides.

[a] X. Pang, H. Du, Prof. Dr. X. Chen, Prof. Dr. X. Wang, Prof. X. Jing
State Key Laboratory of Polymer Physics and Chemistry
Changchun Institute of Applied Chemistry
Chinese Academy of Sciences, 5625 Renmin Street
Changchun 130022 (China)
Fax: (+86) 431-852-65653
E-mail: xschen@ciac.jl.cn

[b] X. Pang, H. Du
Graduate School of Chinese Academy of Sciences
Beijing 100039 (China)

Supporting information for this article is available on the WWW under http://www.chemeurj.org/ or from the author.

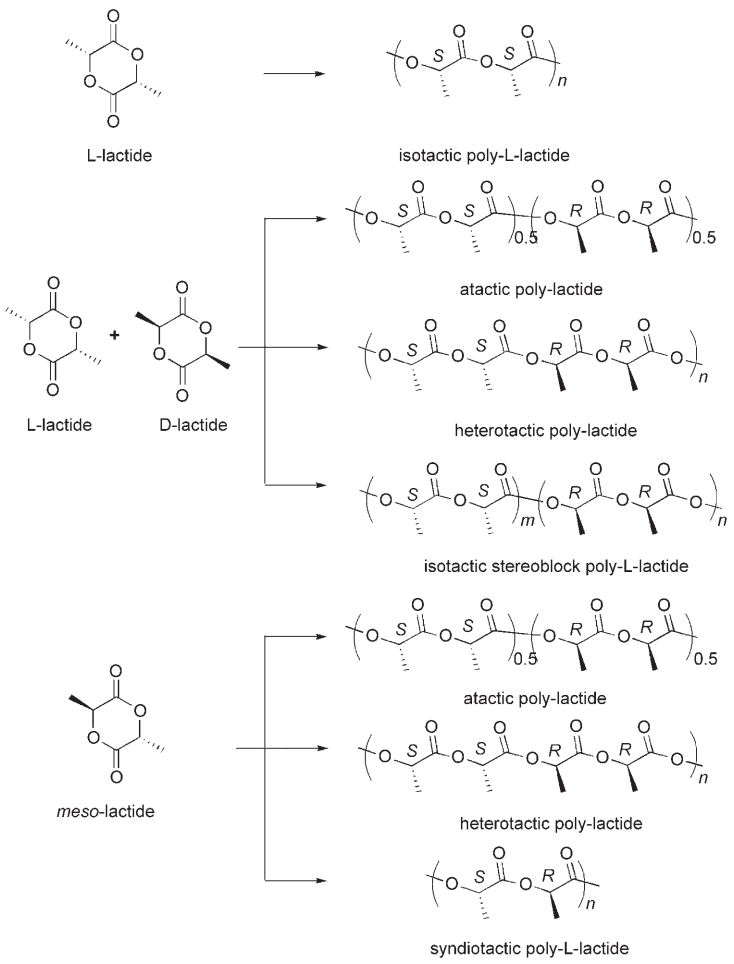

Scheme 2. Microstructures of PLA.

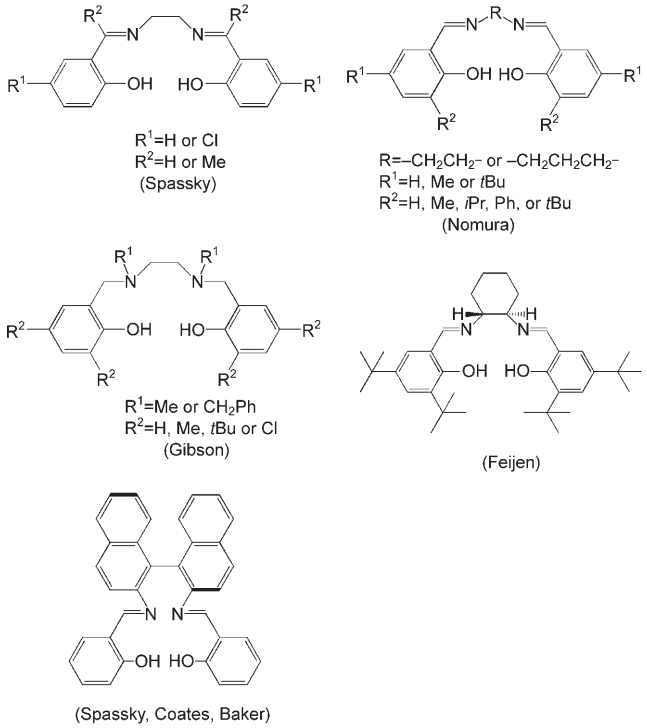

Scheme 3. Ligand precursors explored for stereoselective ROP of lactides.

Since stereocomplex polymers formed by an equivalent mixture of PLLA and PDLA have many advantages such as higher melting temperature (230 °C).[7] Many efforts have been made to obtain crystalline PLA via direct ring-opening polymerization (ROP) of racemic lactide (*rac*-LA; i.e., a 1:1 mixture of L-LA and D-LA) by the stereoselective catalysts. Stereoblock PLA can be obtained from *rac*-LA using the aluminum complex of a chiral binaphthyl Schiff base originally proposed by Spassky et al.[8] A few other excellent studies have attempted to elucidate the relationship between the aluminum Schiff base complexes and stereoselectivity[9] (Scheme 3). Among them, Coates,[9a] Feijen[9c,d] and Duda[9j] used chiral salen-type Schiff base catalysts via the enantiomorphic site control mechanism; Nomura[9e] and our group[9g,h] used achiral salen-type Schiff base catalysts via the chain-end control mechanism.

Enolic ligands could be obtained from the reaction of β-diketone and diamine. Ideal Schiff base ligands and their aluminum complexes can be obtained through keto–enol tautomerism. To the best of our knowledge, few researches on enolic Schiff bases and their metal complexes have been reported in the *rac*-LA polymerization.[10] It is postulated that aluminum complexes coordinated by enolic Schiff base might be a potential catalyst for ROP of *rac*-LA. We recently communicated two enolic Schiff base complexes acting as the precursors for the polymerization of *rac*-LA by a chain end controlled mechanism.[11] To expand our initial work, we have investigated the effect of the complex architecture on the lactide polymerization behavior. We tried to elucidate the relationship between the complex structure and the catalytic performance of the enolic Schiff base aluminum complexes. Our approach was based on fine-tuning of the ancillary ligand and study of the effect on the catalytic reactivity. Herein we systematically explore the synthesis, characterization and stereoselective polymerization of the enolic Schiff base aluminum complexes family.

Results and Discussion

Ligand synthesis: The versatile ligand family (Scheme 4) was easily synthesized from readily available starting materials, namely primary diamines with acetylacetone, 1-benzoylacetone and 1,1,1-trifluoro-acetylacetone.[12]

Ligands **1**, **2** and **7** had the identical aliphatic diimine backbones but the different enol substituents: CH_3 for **1**, C_6H_5 for **2** and CF_3 for **7**. Ligands **2**, **3**, **4** and **5** had identical enol segments but the different diimine backbones: $-CH_2CH_2-$ for **2**, $-CH_2CH_2CH_2-$ for **3**, $-CH_2C(CH_3)_2CH_2-$ for **4** and $-CH_2C_6H_5CH_2-$ for **5**. Ligands **5** and **6** had the identical aryl diimine backbones but the different enol substituents: C_6H_5 for **5** and CH_3 for **6**.

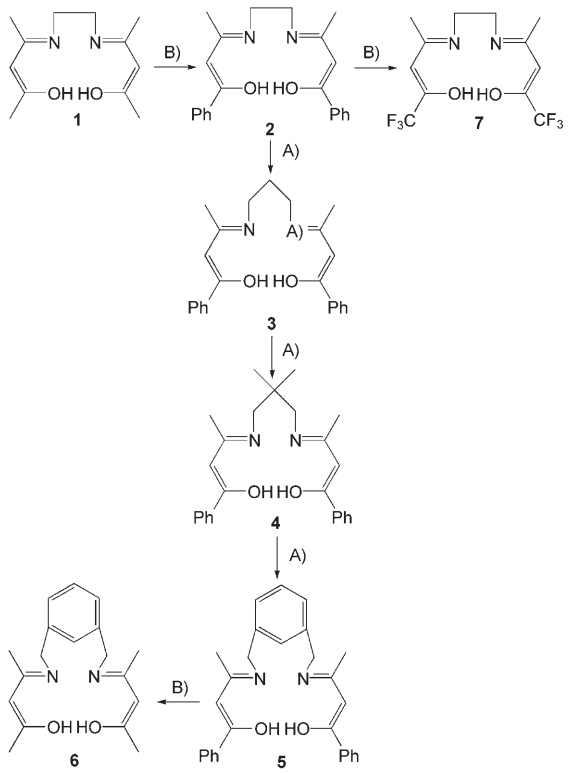

Scheme 4. Ligands prepared for the stereoselective polymerization of lactides. A) change of the diamine substituents, B) change of diketone substituents.

Complex formation and crystal structure characterization: Reaction of ligands **1**–**7** with stoichiometric $AlEt_3$ in toluene formed enolic Schiff base aluminum ethyl complexes **1a**–**7a**, respectively. All these complexes were isolated as solid powders. To estimate the relationship between geometric structures and their catalytic performance, single crystals of **2a**, **3a**, and **4a** were measured (Table 1). X-ray diffraction data showed that all three crystals were five-coordinated around the aluminum center. The parameter τ was used to describe the degree of crystal distortion of a five-coordinated Schiff base aluminum complex:[13] a perfect square-pyramidal geometry (sqp) corresponds to $\tau = 0$, while perfect trigonal bipyramidal geometry (tbp) corresponds to $\tau = 1$.

The molecular structure of **2a** with the τ value of 0.09 was shown in Figure 1. The geometry around the Al atom was sqp geometry with the ethyl group lying on the axial position and two nitrogen atoms and two oxygen atoms on the basal position. Central Al atom was about 0.531 Å above the N1-N2-O1-O2 mean plane with an average compressed axial O1-Al-N2 bond angle of 150.34(15)° and equatorial O2-Al-N1, C23-Al-N1, and O2-Al-C23 bond angles of 144.91(15), 110.24(18), and 104.72(16)°, respectively. The distances from the Al atom to O1, O2, N1, N2 and C23 were 1.831(3), 1.835(3), 1.982(5), 1.999(5) and 1.970(4) Å, respectively. Compound **3a** had a τ value of 0.78, manifesting that **3a** adopted a distorted tbp geometry with O1 and N2 occupying the axial site and O2, N1 and ethyl group lying on the equatorial plane. The central Al atom was about 0.029 Å above the equatorial plane formed by O2, N1 and C1 in the direction of N2 with an average compressed axial O1-Al-N2 bond angle of 167.88(9)° and equatorial O2-Al-N1, C1-Al-N1, and O2-Al-C1 bond angles of 120.41(9), 120.56(11), and 118.96(11)°, respectively. The distances from the Al atom to O1, O2, N1, N2 and C1 were 1.8881(18), 1.8108(19), 1.961(2), 2.081(2) and 1.949(3) Å, respectively.[11] Compound **4a** has an identical τ value (0.78) with **3a**. The geometry of **4a** (Figure 2) was analogous to **3a** with an average compressed axial O2-Al-N1 bond angle of 167.78(6)° and equatorial O1-Al-N2, O1-Al-C15, and N2-Al-C15 bond angles of 120.60(6), 119.25(7) and 120.15(7)°, respectively. The distances from the Al atom to O1, O2, N1, N2 and C15 were 1.8151(12), 1.8724(12), 2.0639(14), 1.9674(15) and 1.9885(18) Å, respectively. Central Al atom was about 0.001 Å above the equatorial plane formed by O1, N2 and C15 in the direction of O2. The difference of the τ values between **2a** and **3a** was presumably due to the nature of their diimine backbones, **3a** had more flexible C_3 backbone than **2a** (C_2 backbone); the tbp geometry in **3a** may avoid the eclipse of methylene hydrogens. The similar results were reported in salen aluminum systems.[13a] The substituent groups in the middle carbon of the C_3 backbone seemed to have no obvious influence in comparison with the diimine backbone length on the geometry as **3a** and **4a** had the same τ value.

Further insight into the nature of real initiators of ROP and the effect of the fifth coordinated group on geometry came from the preparation and characterization of two enolic Schiff base aluminum isopropoxides **2b** and **4b** via in situ alcoholysis (Scheme 5). X-ray single crystal structure analysis of **2b** also showed a five-coordinated aluminum center (Figure 3). The τ value of **2b** was 0.54. The geometry around the Al atom was a distorted tbp geometry with O2 and N1 occupying the axial site and O1, N2 and O3 lying on the equatorial plane. Central Al atom was about 0.088 Å above the equatorial plane formed by O1, N2 and O3 in the direction of O2 with an average compressed axial O2-Al-N1 bond angle of 165.50(7)° and equatorial O1-Al-N2, O1-Al-O3, and N2-Al-O3 bond angles of 133.27(6), 113.05(7) and 112.98(7)°. The distances from the Al atom to O1, O2, N1, N2 and O3 were 1.8217(13), 1.8389(13), 1.9897(16), 1.9827(16) and 1.7443(14) Å. The large difference in the τ values between **2a** (aluminum ethyl, τ value was 0.09) and **2b** (aluminum isopropoxide, τ value was 0.54) manifested that **2b** was more distorted than **2a**. The geometry of **4b** was distorted tbp with O1 and N2 occupying the axial site and O2, N1 and O3 lying on the equatorial plane (Figure 4). Central Al atom was about 0.046 Å above the equatorial plane formed by O2, N1 and O3 in the direction of O1 with an average compressed axial O1-Al1-N2 bond angle of 172.87(14)° and equatorial O2-Al1-N1, O2-Al1-O3, and N1-Al1-O3 bond angles of 120.31(14), 121.83(14) and 117.67(14)°, respectively. The distances from the Al1 atom to O1, O2, N1, N2 and O3 were 1.861(3), 1.802(3), 1.967(3), 2.011(4) and 1.740(3) Å, respectively. The τ value of **4b** was

Table 1. Crystallographic data for **2a**, **3a**, **4a**, **2b** and **4b**.[a]

	2a	**3a**	**4a**	**2b**	**4b**
empirical formula	$C_{24}H_{27}AlN_2O_2$	$C_{25}H_{29}AlN_2O_2$	$C_{27}H_{33}AlN_2O_2$	$C_{25}H_{29}AlN_2O_3$	$C_{70}H_{86}Al_2N_4O_6$
formula weight	402.46	416.48	444.53	432.48	1133.39
T [K]	187(2)	187(2)	187(2)	187.0(2)	187(2)
λ [Å]	0.71073	0.71073	0.71073	0.71073	0.71073
crystal system	monoclinic	monoclinic	monoclinic	triclinic	monoclinic
space group	$P2_1/n$	$C2/c$	$P2_1/n$	$P\bar{1}$	Cc
a [Å]	7.4501(6)	29.660(3)	9.9827(7)	10.4661(11)	22.4239(14)
b [Å]	18.6477(16)	7.5901(6)	11.1884(8)	10.6923(11)	13.4238(8)
c [Å]	15.5635(14)	22.3793(19)	21.7980(16)	12.2855(13)	21.9046(14)
α [°]	90	90	90	86.341(2)	90
β [°]	98.712(2)	116.486(2)	96.1190(10)	66.2050(10)	102.7490(10)
γ [°]	90	90	90	64.0240(10)	90
V [Å^3], Z	2137.2(3), 4	4509.4(7), 8	2420.8(3), 4	1120.2(2), 2	6431.0(7), 4
ρ_{calcd} [Mg m^{-3}]	1.251	1.227	1.220	1.282	1.171
μ [mm^{-1}]	0.117	0.113	0.110	0.120	0.099
F(000)	856	1776	952	460	2432
crystal size [mm]	0.36×0.11×0.10	0.41×0.15×0.06	0.50×0.21×0.15	0.53×0.13×0.03	0.27×0.25×0.19
θ range [°]	1.72 to 25.25	1.53 to 26.05	1.88 to 26.00	1.83 to 25.50	1.78 to 26.04
limiting indices (hkl)	−7 to 8	±36	−11 to 12	−9 to 12	−27 to 13
	−21 to 22	±9	±13	±12	±16
	±18	−21 to 27	−26 to 13	±14	−26 to 27
reflections collected	11693	12309	13302	6077	17895
independent reflections	3855	4434	4766	4093	8412
R_{int}	0.0455	0.0500	0.0229	0.0160	0.0299
goodness of fit on F^2	1.015	1.037	1.036	1.017	1.009
final $R1$, $wR2$ [$I>2\sigma(I)$]	0.0825, 0.1696	0.0613, 0.1305	0.0438, 0.1138	0.0431, 0.1061	0.0533, 0.1348
$R1$, $wR2$ (all data)	0.1243, 0.1932	0.0981, 0.1489	0.0536, 0.1214	0.0566, 0.1151	0.0709, 0.1483
largest diff. peak and hole [e Å^{-3}]	0.385, −0.404	0.353, −0.276	0.315, −0.197	0.311, −0.210	0.406, −0.227

[a] Selected bond lenths and angles are available in the Supporting Information.

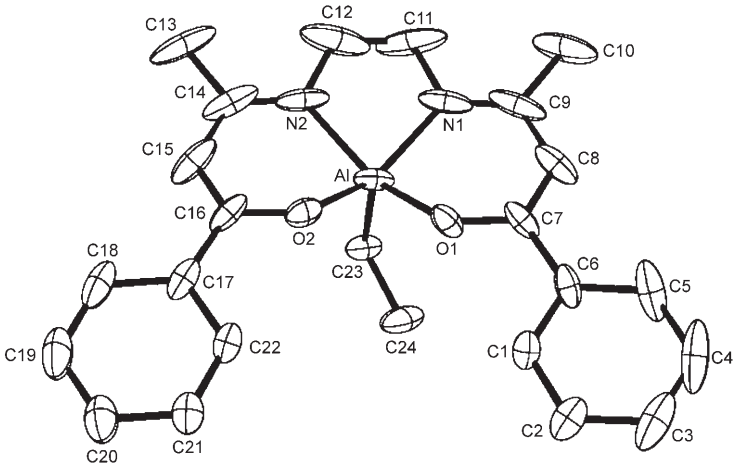

Figure 1. Crystal structure of complex **2a**.

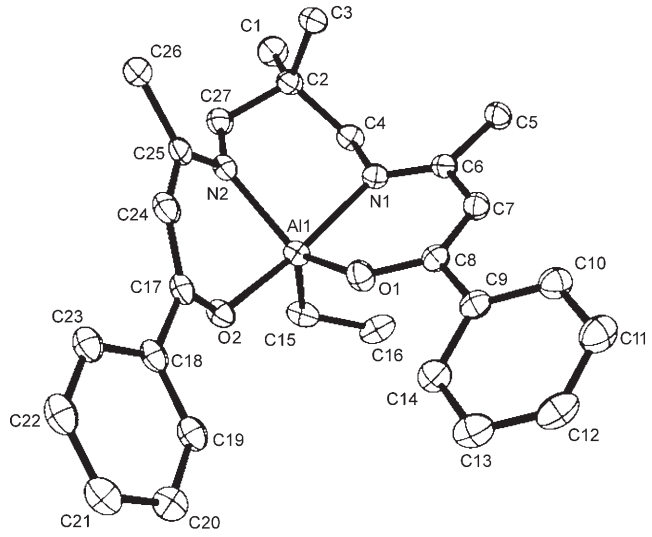

Figure 2. Crystal structure of complex **3a**.

0.85. Compound **4b** showed more tbp geometry character than **4a** (τ value was 0.78). From the crystal analysis, it was believed that the fifth coordinated group had notable influence on the complex's geometry.

Complexes structure characterization in solution: Although the solid-state structures of these complexes showed monomeric behavior, we could not conclude whether these complexes retained their monomeric structures in their solution-state. Coates et al.[9a] reported that the salen-type aluminum isopropoxide, which had less steric hindrance, had a dimer character in the solution state, though the dimer was inactive in the lactide polymerization. Recently, Lin et al.[14] reported that the Schiff base zinc complex showed dimer behavior in the solid state, but in the solution state, a mixture of dimer and monomer (include diastereoisomer) was observed. In order to determine the real conformation of these complexes in the solution state, we investigated the ^{1}H and ^{27}Al NMR spectra of these complexes. The ^{1}H NMR spectra of the ethyl complexes **1a**–**7a** showed one set of resonance peak and the ^{27}Al NMR spectra of **1a**–**7a** showed resonance peak at about 36 ppm, indicating that all the ethyl complexes retained their conformation with the five-coordinated monomeric Al center in the solution state.[15] The ^{1}H NMR spectra of the isopropoxide complexes **2b** and **4b** also showed one set of resonance peak; additional ^{27}Al spectra showed a resonance peak at about 36 ppm. We could conclude from

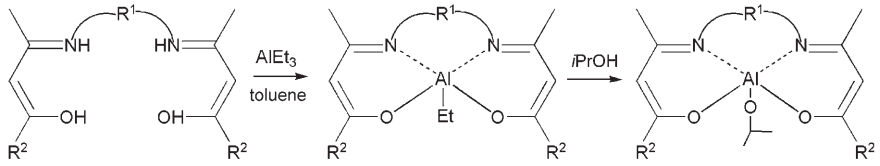

Scheme 5. Synthetic pathway for the preparation of complexes.

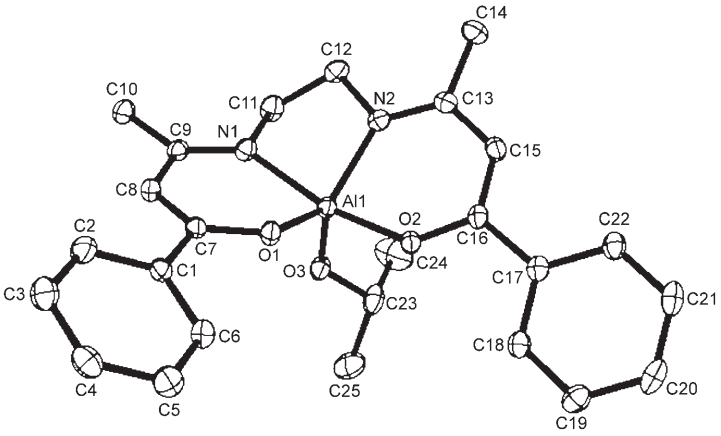

Figure 3. Crystal structure of complex **2b**.

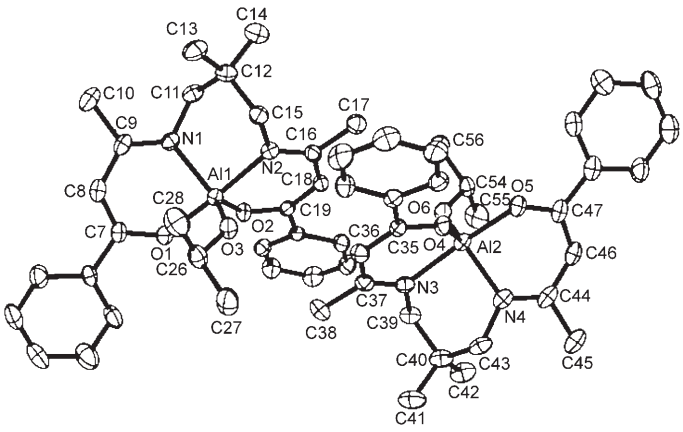

Figure 4. Crystal structure of complex **4b**.

the spectral results that both **2b** and **4b** retained the five-coordinated monomeric Al center as in the solid structure.

Kinetic studies: The polymerization processes were investigated by kinetic studies using **1a**–**7a**. Polymerization data were collected in Table 2. The data of conversion versus time were collected for both the aliphatic diimine backbone complexes (**1a**, **2a**, **3a**, **4a** and **7a**)[17] and aryl diimine backbone complexes (**5a** and **6a**), respectively (Figures 5 and 6). First-order kinetics in monomer was observed [Eq. (1)], where k_{app} was the apparent polymerization rate constant.

$$\frac{-\mathrm{d}[\mathrm{LA}]}{\mathrm{d}t} = k_{app}[\mathrm{LA}] \quad (1)$$

The number-average molecular weight (M_n) also followed a linear relationship in monomer conversion for both the aliphatic diimine backbone complexes (Figure 7) and aryl diimine backbone complexes (Figure 8). The molecular control and the low polydispersity indicated that the polymerization had a characteristic of controlled propagation. To determine the order in Al, k_{app} was plotted versus the concentration of Al (Figure 9) using **4a**. From this plot, k_{app} increased linearly with the Al concentration, manifesting that the order in Al was first-order too. Therefore, the polymerization of *rac*-LA using **4a** followed an overall kinetic equation of the form as Equation (2), where k_p was the polymerization rate constants and $k_p = k_{app}/[\mathrm{Al}]$.

$$\frac{-\mathrm{d}[\mathrm{LA}]}{\mathrm{d}t} = k_p[\mathrm{LA}][\mathrm{Al}] \quad (2)$$

We could extrapolate this equation to other complexes in the *rac*-LA polymerization. Aluminum isopropoxides **2b** and **4b** were also used as real initiators to investigate their reactivities (Table 3). According to the polymerization data, it was concluded that in the present of 2-propanol, aluminum ethyl complex **2a** and aluminum isopropoxide **2b** had same reactivities, similar results were obtained for **4a** and **4b**. It was envisioned that the in situ alcoholysis reaction of aluminum ethyl complex with 2-propanol were almost quantitative (Scheme 5). The ^{1}H NMR spectrum of the LA oligomers indicated that the polymer chains were end-capped with an isopropyl ester and a hydroxyl group[11] and the ring-opening occurred through a so-called coordination–insertion mechanism[18] as described in Scheme 6. Because the complexes in this paper had no chirality, it was presumed that the polymerization followed a so-called chain-end control mechanism.[9e,19,20]

The influence of temperature on the polymerization rate was investigated (Figure 10). The polymerization rate increased with the increasing temperature, but the stereoselectivity decreased. Determination of the stereochemical microstructures of PLA was achieved through inspection of the methine region of homonuclear decoupled ^{1}H NMR spectra of the resultant polymers.[9a,c,11] The apparent polymerization rate constant (k_{app}), polymerization rate constants (k_p) and P_m[21] values are collected in Table 4. With these three parameters, the activation energy of the polymerization was calculated by fitting them to the Arrhenius equation ($k_p = Ae^{-E_a/RT}$): an activation energy E_a of 35.4 kJ mol^{-1} was deduced by plotting $\ln k_p$ versus $1/T$. The activation energy for **4a** was much lower compared with that with tin(II) octanoate (70.9 ± 1.5 kJ mol^{-1}).[22]

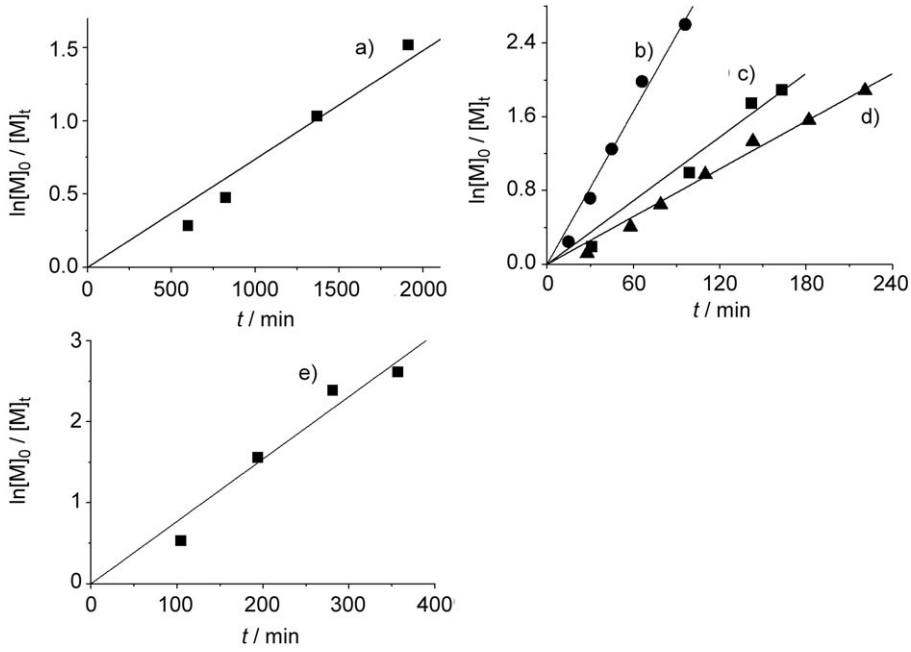

Figure 5. Kinetic plots of the *rac*-lactide conversion vs. the reaction time: a) complex **1a**/2-propanol, $[M]_0/[Al]=65$; b) complex **4a**/2-propanol, $[M]_0/[Al]=40$; c) complex **4a**/2-propanol, $[M]_0/[Al]=80$; d) complex **4a**/2-propanol, $[M]_0/[Al]=110$; e) complex **7a**/2-propanol, $[M]_0/[Al]=65$.

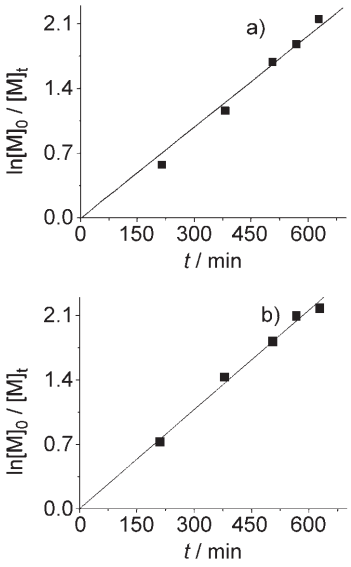

Figure 6. Kinetic plots of the *rac*-lactide conversion vs. the reaction time: a) complex **5a**/2-propanol, $[M]_0/[Al]=56$; b) complex **6a**/2-propanol, $[M]_0/[Al]=56$.

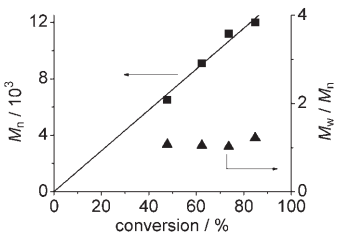

Figure 7. Plot of PLA M_n and polydispersity (M_w/M_n) as a function of *rac*-lactide conversion using complex **4a**/2-propanol, $[M]_0/[Al]=110$.

Complex structure and stereoselective polymerization

Effect of the diimine backbone length and substituent: Complexes **2a**, **3a**, **4a** and **5a** have an identical enol structure but different diimine backbones. Correspondingly, they displayed different catalytic behaviors (Table 2 entry 2, 3, 4 and 5). Lengthening the backbone from C_2 to C_3 gave rise to significant increase in activity. Compound **2a** had C_2 backbone while **3a** had C_3 backbone; the catalytic activity of **3a** was much higher than that of **2a**.[11] Apparently, the C_3 backbone had a positive effect on the polymerization rate. Probably the higher backbone flexibility was suitable for the metal coordination sphere to open the inserting monomer ring. To further investigate the effect of backbone on the catalytic activity, modification in the backbone of **3a** was produced. The dimethyl-substituted complex **4a** had the highest activity. The k_p value for **4a** ($1.90\ L\,mol^{-1}\,min^{-1}$) was much higher than those of **2a** ($0.19\ L\,mol^{-1}\,min^{-1}$) and **3a** ($0.26\ L\,mol^{-1}\,min^{-1}$). Clearly the *gem*-methyls in **4a** were the reason for the remarkable change in activity between **3a** and **4a**, presumably due to the *gem*-methyls made the aluminum–oxygen bond easier to cleave when coordinated with the monomer resulting in higher activity. Therefore, it could be concluded that the aliphatic diimine backbone length and substituent had remarkable influence on the complex's activity. Similar phenomenon was reported by Nomura[9l] and our group[9g] for the salen-type catalysts: catalyst possessing 2,2-dimethyl-1,3-propanediimine backbone was more active than that possessing 1,3-propanediimine backbone. Complex **5a** had the lowest stereoselectivity ($P_m=0.58$) among the four complexes. It was assumed that because the aliphatic backbone was more flexible than aryl analogues and therefore it could provide more steric hindrance during the insertion of monomer. Due to the planar aryl diimine backbone and the lack of enough steric hindrance, aryl analogues would have lower stereoselectivity.

Complexes **4a** and **3a** had the same τ value (0.78), while **2a** had 0.09. It manifested that **3a** and **4a** were closer to the tbp geometry than **2a**. By comparing the τ values and the stereoselectivity, maybe further deduction concerning the geometry and the stereoselectivity could be made, that is, the sqp geometry of a complex did not benefit the stereoselective polymerization of *rac*-lactides, and complexes containing higher τ values (closer to tbp geometry) would have

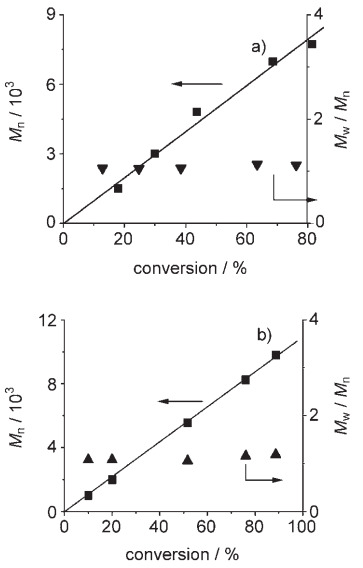

Figure 8. Plot of PLA M_n and polydispersity (M_w/M_n) as a function of *rac*-lactide conversion using a) complex **5a**/2-propanol, $[M]_0/[Al]=56$; b) complex **6a**/2-propanol, $[M]_0/[Al]=56$.

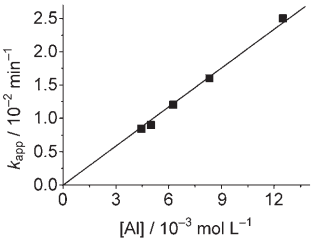

Figure 9. k_{app} vs. the concentration of **4a**/2-propanol initiator for the *rac*-LA polymerization.

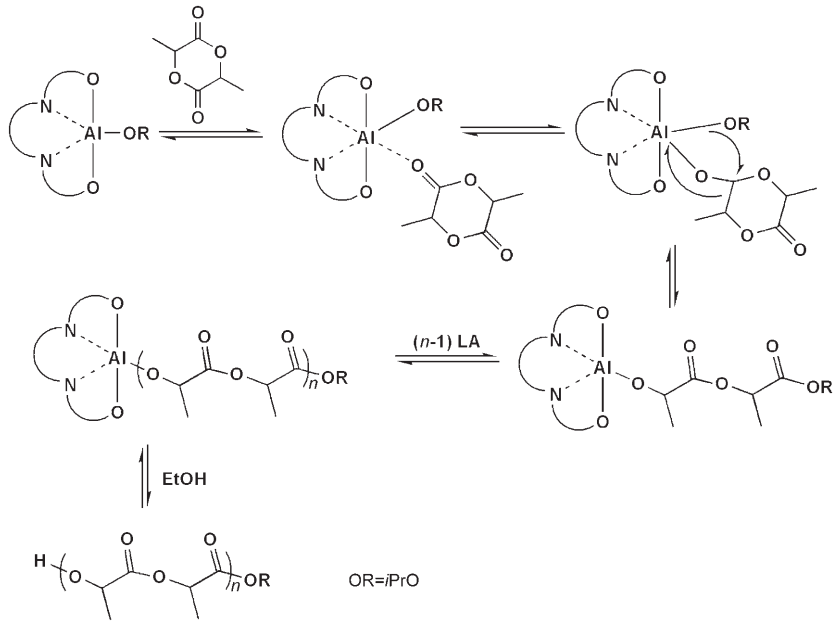

Scheme 6. Proposed mechanism for the polymerization of lactides using enolic Schiff base aluminum isopropoxides.

higher stereoselectivity. We temporarily assumed that the complex containing the tbp geometry had positive synergic effect to retain and extend the chirality caused by the chiral monomer after the insertion. The tbp geometry effect made the chiral recognition of incoming monomer more effective, whereas the sqp geometry did not possess this character.[23] A similar phenomenon was reported by Nomura[9l] and our group[9g] for the salen-type catalysts.

Lin et al.[14] reported that the stronger metal alkoxide bond would have a slower reaction rate in the ROP of lactide compared with the Schiff base zinc complex. It was not the case in our systems, since **2b** and **4b** had almost equal aluminum alkoxide bone length [1.7443(14) for **2b** and 1.740(3) for **4b**] but their polymerization rate differed considerably (Table 3).

Effect of the enol substituent: Complexes **1a**, **2a** and **7a** had the same diimine backbone, but different enol substituents. Complex **7a** had the highest activity and the highest stereoselectivity among the three complexes (Table 2, entries 1, 2 and 7). An electronic effect was obvious, with electron-withdrawing substituents in the enol segments affording more active aluminum centers, presumably a consequence of enhanced metal electrophilicities. Hence, the fluorine-substituted complexes typically exhibit greater polymerization activities than do their counterparts bearing unsubstituted enol segments. Similar conclusion were reported by Gibson[9k] that chloro substituents in the phenoxide unit had higher activity and higher stereoselectivity than their dimethyl analogues for salan-type catalysts. The increased selectivity suggested that the electron-withdrawing groups did not take a direct but a complicated way to affect the complex's behavior during the polymerization for both salan-type catalysts and enolic complexes. The effect of substituent from methyl group to phenyl group was not remarkable in comparison with the diimine substituents (Table 2, entries 1 and 2). Complexes **1a** and **2a** had the similar activity and stereoselectivity, and the similar results were observed for aryl backbone complexes **5a** and **6a** (Table 2, entries 5 and 6).

Stereochemistry of rac-LA: In the case of random propagation (Bernoullian statistics), the additions of different enantiomeric monomers were independent events, the different rate constants were equal. Since the ligands and complexes reported were achiral, and there was a preference for isotactic addition during the

Table 2. Polymerization data of *rac*-LA using complexes **1a**–**7a** at 70 °C in toluene.[a]

Entry	Complex	t [min]	$[M]_0/[I]$	Conv.[b] [%]	M_n(calcd)[c] [10^{-3}]	M_nGPC[d] [10^{-3}]	PDI[d]	k_p[e]	P_m
1	**1a**	1927	65	78	7.3	13.2	1.39	0.11	0.68
2	**2a**	1506	65	87	8.2	12.8	1.15	0.19	0.69
3	**3a**	551	65	85	8.0	15.7	1.09	0.26	0.75
4	**4a**	127	65	88	8.2	16.2	1.04	1.90	0.78
5	**4a**	221	110	80	12.7	21.5	1.02	1.90	0.78
6	**5a**	507	56	81	6.5	13.2	1.12	0.36	0.58
7	**6a**	628	56	89	7.2	16.5	1.19	0.41	0.57
8	**7a**	281	65	93	8.7	14.5	1.32	0.92	0.75

[a] All polymerizations were carried out in toluene solution at 70 °C. $[LA]_0 = 0.5\ mol\,L^{-1}$. [b] Measured by ^1H NMR. [c] Calculated from the molecular weight of $LA \times [M]_0/[I] \times$ conversion + M_w(*i*PrOH). [d] Obtained from GPC analysis and calibrated against polystyrene standard. The true value of M_n could be calculated according to formula $M_n = 0.58\,M_{n\,GPC}$.[16] [e] k_p($L\,mol^{-1}\,min^{-1}$): Calculated from the relationship $k_p = k_{app}/[Al]$.

Table 3. Polymerization data of *rac*-LA using complexes **2b** and **4b** in toluene.[a]

Entry	Complex	t [min]	$[M]_0/[I]$	Conv.[b] [%]	M_n(calcd)[c] [10^{-3}]	$M_{n\,GPC}$[d] [10^{-3}]	PDI[d]	P_m
1	**2b**	1528	65	90	8.4	13.5	1.14	0.68
2	**2b**	2140	75	93	10.1	14.7	1.20	0.66
3	**4b**	96	40	93	12.8	23.5	1.03	0.78
4	**4b**	140	65	90	8.4	16.3	1.05	0.78
5	**4b**	230	110	85	12.8	23.5	1.03	0.78
6	**4b**	335	150	90	19.5	36.8	1.04	0.78

[a] All polymerizations were carried out in toluene solution at 70 °C, $[LA]_0 = 0.5\ mol\,L^{-1}$. [b] Measured by ^1H NMR. [c] Calculated from the molecular weight of $LA \times [M]_0/[I] \times$ conversion + M_w(*i*PrOH). [d] Obtained from GPC analysis and calibrated against polystyrene standard. The true value of M_n could be calculated according to formula $M_n = 0.58\,M_{n\,GPC}$.[16]

Table 4. Kinetic results of *rac*-LA polymerization at different temperatures using **4a**/2-propanol in toluene, $[M]/[I] = 110$.

T [°C]	k_{app} [min^{-1}]	k_p [$L\,mol^{-1}\,min^{-1}$]	P_m
70	0.0086	1.90	0.78
90	0.0141	3.11	0.73
110	0.0318	6.99	0.69

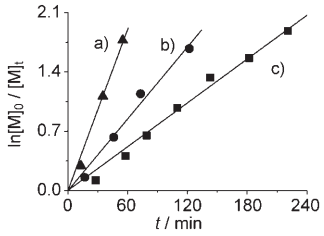

Figure 10. Kinetics of the *rac*-LA polymerization using **4b** at the reaction temperatures of a) 110 °C; b) 90 °C; c) 70 °C, $[M]_0/[Al] = 110$.

ROPs of *rac*-LA, we considered the chain-end control mechanism.[9e,19,20] In such a reaction, the ligand and the complex were achiral; the initiation reaction occurred without any differentiation between the two enantiomers, and the last unit in the growing polymer chain influenced which enantiomer form of the monomers would incorporate next. So we would prefer a first-order Markovian statistics[24–26] rather than a Bernoullian statistics in such a mode of propagation. PLA derived from *rac*-lactide could exhibit up to five tetrad sequences (mmm, mmr, rmm, mrm, rmr) in relative ratios determined by the ability of initiators to control racemic [r-diad] and meso [m-diad] connectivity of the monomer units. According to first-order Markovian statistics, the probability for *meso* linkages could be determined as

$$\begin{aligned} P_m &= k_m/(k_m + k_r) \\ &= k_{S/SS}/(k_{S/SS} + k_{S/RR}) \\ &= k_{R/RR}/(k_{R/SS} + k_{R/RR}) \end{aligned} \quad (3)$$

where $k_{S/SS}$ and $k_{R/RR}$ were the rate constants of homo-propagation, $k_{S/RR}$ and $k_{R/SS}$ were the rate constants of cross-propagation. If $k_{S/SS} > k_{S/RR}$ or $k_{R/RR} > k_{R/SS}$, the formation of isotactic sequences were favored, otherwise syndiotactic sequences were formed. The following equations could be deduced according to absolute reaction rate theory:

$$k_{S/SS} = k_{R/RR} = k_m = (kT/h)\exp[(\Delta S^{\neq}_{,m}/R) - (\Delta H^{\neq}_{,m}/RT)] \quad (4)$$

$$k_{R/SS} = k_{S/RR} = k_r = (kT/h)\exp[(\Delta S^{\neq}_{,r}/R) - (\Delta H^{\neq}_{,r}/RT)] \quad (5)$$

Further deduction of equation 6 could be obtained from Equations (4) and (5):

$$\begin{aligned} &P_m/(1-P_m) = k_m/k_r \\ &= \exp[(\Delta S^{\neq}_{,m} + \Delta S^{\neq}_{,r})/R - (\Delta H^{\neq}_{,m} - \Delta H^{\neq}_{,r})/RT] \end{aligned} \quad (6)$$

where $(\Delta S^{\neq}_{,m} - \Delta S^{\neq}_{,r})$ was the entropy difference between homo-propagation and cross-propagation, and $(\Delta H^{\neq}_{,m} - \Delta H^{\neq}_{,r})$ was the enthalpy difference between homo-propagation and cross-propagation. To determine the different values of $(\Delta S^{\neq}_{,m} - \Delta S^{\neq}_{,r})$ and $(\Delta H^{\neq}_{,m} - \Delta H^{\neq}_{,r})$, $\ln P_m/(1-P_m)$ was plotted versus the $1/T$ (Figure 11). From this plot, the entropy difference $(\Delta S^{\neq}_{,m} - \Delta S^{\neq}_{,r})$ of $-26.6 \pm 2.3\ cal\,K^{-1}\,mol^{-1}$ and activation enthalpy difference $(\Delta H^{\neq}_{,m} - \Delta H^{\neq}_{,r})$ of $-12.7 \pm 0.8\ kcal\,K^{-1}\,mol^{-1}$ were obtained, which may explain the preference of isotactic stereosequence.

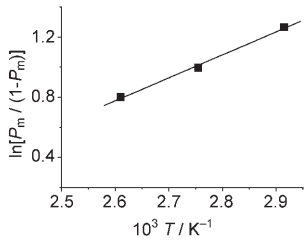

Figure 11. Relationship between polymerization temperature and stereochemistry of the resulting poly(*rac*-LA)s by using **4a**/2-propanol.

Conclusion

We have synthesized a series of five-coordinated enolic Schiff base aluminum complexes derived from β-diketone and diamine. Their catalytic behavior in racemic-lactide polymerization varied remarkably. A plausible mechanism of polymerization was proposed. Complex **4b** had the highest activity and stereoselectivity among all complexes. The different performance of these complexes was attributed to the different diimine backbone and diketone substituent groups on auxiliary ligands. There was a combinatorial effect of electronic and steric factors. Because the complexes in this paper had no chirality, it was presumed that the polymerization followed a so-called chain-end control mechanism. Researches toward the origin of the activity and stereoselectivity of enolic Schiff base aluminum complexes are currently in progress.

Experimental Section

General: All experiments were carried out under argon using Schlenk techniques. Starting materials for the synthesis of ligand **1–7** were purchased from Aldrich Inc. and used without further purification. Toluene was distilled from Na/benzophenone. Ethyl acetate and 2-propanol were distilled from CaH_2 under the protection of argon. *rac*-Lactide (Purac) was purified by recrystallization from ethyl acetate and dried under vacuum at room temperature (RT) before use. NMR spectra were recorded on Bruker AV 300 M and Bruker AV 400 M in $CDCl_3$ at 25 °C. Chemical shifts were given in parts per million from tetramethylsilane. Gel permeation chromatography (GPC) measurements were conducted with a Waters 515 GPC with $CHCl_3$ as the eluent (flow rate: 1 mL min^{-1}, at 35 °C). The molecular weights were calibrated against polystyrene (PS) standards. Crystallographic data were collected on a Bruker APEX CCD diffractometer with graphite-monochromated $Mo_{K\alpha}$ radiation (λ = 0.71073 Å) at 187 K. The structure was refined by the full-matrix least-squares method on F^2 using the SHELXTL-97 crystallographic software package. Anisotropic thermal parameters were used to refine all nonhydrogen atoms. Hydrogen atoms were located in idealized positions.

Ligand synthesis (General Procedure): A solution of diamine (0.1 mol L^{-1}) in ethanol (50 mL) was added dropwise to a stirred solution of diketone (0.2 mol L^{-1}) in ethanol (50 mL). The reaction mixture was refluxed for 14 h before cooling to RT. After removal of the solvent under vacuum a crystalline solid was produced and purified by recrystallization in ethanol.

Ligand 1: Ligand **1** was obtained as a white crystalline solid in 85% yield. ^{1}H NMR (400 MHz, $CDCl_3$): δ = 5.00 (s, 2H, CHCOH), 3.43 (d, 4H, N(CH_2CH_2)N), 2.00 (s, 6H, CH_3COH), 1.91 ppm (s, 6H, CH_3CN); ^{13}C NMR (100 MHz, $CDCl_3$): δ = 194.8 (CH_3COH), 162.7 (CH_3CN), 95.8 (CHCOH), 43.4 (NCH_2), 28.6 (CH_3COH), 18.4 ppm (CH_3CN); elemental analysis calcd (%) for $C_{12}H_{20}N_2O_2$: C 64.26, H 8.99, N 12.49; found: C 64.52, H 9.20, N 12.38.12.

Ligand 2: Ligand **2** was obtained as a white crystalline solid in 80% yield. ^{1}H NMR (400 MHz, $CDCl_3$): δ = 7.86 (d, 4H, ArH), 7.42 (m, 6H, ArH), 5.75 (s, 2H, CHCOH), 3.61 (d, 4H, N(CH_2CH_2)N), 2.09 ppm (s, 6H, CH_3CN); ^{13}C NMR (100 MHz, $CDCl_3$): δ = 188.2 (ArCOH), 164.7 (CH_3CN), 140.1, 130.5, 128.1, 126.8 (ArC), 92.9 (CHCOH), 43.7 (NCH_2), 19.1 ppm (CH_3CN); elemental analysis calcd (%) for $C_{22}H_{24}N_2O_2$: C 75.83, H 6.94, N 8.04; found: C 75.97, H 7.21, N 8.11.

Ligand 3: Ligand **3** was obtained as a white crystalline solid in 77% yield. ^{1}H NMR (400 MHz, $CDCl_3$): δ = 7.87 (d, 4H, Ar*H*), 7.43 (m, 6H, Ar*H*), 5.70 (s, 2H, C*H*COH), 3.53 (m, 4H, N(C$H_2$$CH_2CH_2$)N), 2.17 (s, 6H, CH_3CN), 2.04 ppm (t, 2H, N($CH_2CH_2CH_2$)N); ^{13}C NMR (100 MHz, $CDCl_3$): δ = 187.7 (ArCOH), 164.9 (CH_3CN), 140.1, 130.3, 128.0, 126.7 (ArC), 92.3 (CHCOH), 39.8 (N($CH_2CH_2CH_2$)N), 29.9 (N($CH_2CH_2CH_2$)N), 19.1 ppm (CH_3CN); elemental analysis calcd (%) for $C_{23}H_{26}N_2O_2$: C 76.21, H 7.23, N 7.73; found: C 76.19, H 7.21, N 7.86.

Ligand 4: Ligand **4** was recrystallized in hexane and obtained as a white crystalline solid in 51% yield. ^{1}H NMR (400 MHz, $CDCl_3$): δ = 7.85 (d, 4H, ArH), 7.41 (m, 6H, ArH), 5.70 (s, 2H, CHCOH), 3.30 (d, 4H, N($CH_2C(CH_3)_2CH_2$)N), 2.06 (s, 6H, CH_3CN), 1.20 ppm (s, 6H, N($CH_2C(CH_3)_2CH_2$)N); ^{13}C NMR (100 MHz, $CDCl_3$): δ = 187.7 (ArCOH), 165.1 (CH_3CN), 140.2, 130.3, 128.0, 126.7 (ArC), 92.3 (CHCOH), 50.4 (N($CH_2C(CH_3)_2CH_2$)N), 35.6 (N($CH_2C(CH_3)_2CH_2$)N), 23.5 (N($CH_2C(CH_3)_2CH_2$)N), 19.3 ppm (CH_3CN); elemental analysis calcd (%) for $C_{25}H_{30}N_2O_2$: C 76.89, H 7.74, N 7.17; found: C 77.05, H 7.65, N 7.22.

Ligand 5: Ligand **5** was obtained as a yellow crystalline solid in 76% yield. ^{1}H NMR (400 MHz, $CDCl_3$): δ = 7.92 (d, 4H, ArH), 7.47 (m, 8H, ArH), 7.26 (s, 2H, ArH), 5.72 (s, 2H, CHCOH), 4.60 (d, 4H, $NCH_2C_6H_4CH_2N$), 2.11 ppm (s, 6H, CH_3CN); ^{13}C NMR (100 MHz, $CDCl_3$): δ = 188.4 (ArCOH), 165.3 (CH_3CN), 140.7, 139.0, 131.0, 130.0, 128.6, 127.6, 126.5, 125.9 (ArC), 93.1 (CHCOH), 47.3 ($NCH_2C_6H_4CH_2N$), 19.9 ppm (CH_3CN); elemental analysis calcd (%) for $C_{28}H_{28}N_2O_2$: C 79.22, H 6.65, N 6.60; found: C 78.96, H 6.56, N 6.46.

Ligand 6: Ligand **6** was obtained as a yellow crystalline solid in 72% yield. ^{1}H NMR (400 MHz, $CDCl_3$): δ = 7.35 (t, 1H, ArH), 7.21 (d, 2H, ArH), 7.15 (s, 1H, ArH), 5.08 (s, 2H, CHCOH), 4.49 (d, 4H, $NCH_2C_6H_4CH_2N$), 2.06 (s, 6H, CH_3COH), 1.94 ppm (s, 6H, CH_3CN); ^{13}C NMR (100 MHz, $CDCl_3$): δ = 195.4 (CH_3COH), 163.2 (CH_3CN), 139.1, 129.6, 126.1, 125.4 (ArC), 96.2 (CHCOH), 46.8 ($NCH_2C_6H_4CH_2N$), 29.2 (CH_3COH), 19.1 ppm (CH_3CN); elemental analysis calcd (%) for $C_{18}H_{24}N_2O_2$: C 71.79, H 8.05, N 9.33; found: C 71.92, H 7.89, N 9.20.

Ligand 7: Ligand **7** was obtained as a yellow crystalline solid in 63% yield. ^{1}H NMR (400 MHz, $CDCl_3$): δ = 5.43 (s, 2H, CHCOH), 3.68 (d, 4H, N(CH_2CH_2)N), 2.15 ppm (s, 6H, CH_3CN); ^{13}C NMR (100 MHz, [D_6]DMSO): δ = 174.9 (CF_3COH), 171.2 (CH_3CN), 118.0 (CF_3COH), 89.2 (CHCOH), 43.6 (NCH_2CH_2N), 18.7 ppm (CH_3CN); ^{19}F NMR (400 MHz, $CDCl_3$): δ = −0.40 ppm (s, 6F); elemental analysis calcd (%) for $C_{12}H_{14}F_6N_2O_2$: C 43.38, H 4.25, N 8.43; found: C 43.62, H 4.38, N 8.60.

Complex synthesis (General Procedure): For enolic Schiff base aluminum ethyl complexes **1a–7a**, $AlEt_3$ (0.2 mmol) in toluene (5 mL) was added to the stirred 1 mL toluene solution of ligand precursors **1–7** (0.2 mmol) at RT. The reaction was maintained at 80 °C for 12 h, and the reaction mixture was then slowly cooled to RT. The toluene was removed under vacuum. For enolic Schiff base aluminum isopropoxides, **2b** and **4b** were prepared by mixing the corresponding ethyl complexes with 2-propanol in toluene solution, the mixture was stirred at 80 °C for 10 h and then slowly cooled to RT. The toluene was removed under vacuum. Crystals suitable for X-ray diffraction were grown from a mixture of toluene and pentane at −10 °C. The crystallographic data and the results of refinements were summarized in Table 1.

Complex 1a: Obtained as a white solid in 95% yield. ^{1}H NMR (400 MHz, $CDCl_3$): δ = 5.02 (s, 2H, CHCOAl), 3.50 (m, 2H, N(CH_2CH_2)N), 3.42 (m, 2H, N(CH_2CH_2)N), 2.03 (s, 6H, CH_3COAl),

1.96 (s, 6H, CH_3CN), 0.85 (t, 3H, $AlCH_2CH_3$), −0.39 ppm (q, 2H, $AlCH_2CH_3$); ^{13}C NMR (100 MHz, $CDCl_3$): δ = 179.4 (CH_3COAl), 171.4 (CH_3CN), 98.8 (CHCOH), 45.7 (NCH_2), 25.5 (CH_3COAl), 21.3 (CH_3CN), 13.6 ($AlCH_2CH_3$), 9.6 ppm ($AlCH_2CH_3$); elemental analysis calcd (%) for $C_{14}H_{23}AlN_2O_2$: C 60.41, H 8.33, N 10.06; found: C 60.20, H 8.61, N 9.87.

Complex 2a: Obtained as a yellow solid in 93% yield. ^1H NMR (400 MHz, $CDCl_3$): δ = 7.90 (d, 4H, ArH), 7.32 (m, 6H, ArH), 5.71 (s, 2H, CHCOAl), 3.53 (m, 2H, $N(CH_2CH_2)N$), 3.45 (m, 2H, $N(CH_2CH_2)N$), 2.04 (s, 6H, CH_3CN), 0.81 (t, 3H, $AlCH_2CH_3$), −0.38 ppm (q, 2H, $AlCH_2CH_3$); ^{13}C NMR (75 MHz, $CDCl_3$): δ = 173.6 (ArCOH), 172.3 (CH_3CN), 138.8, 129.9, 128.0, 126.9 (ArC), 96.6 (CHCOAl), 46.4 (NCH_2), 22.4 (CH_3CN), 10.1 ppm ($AlCH_2CH_3$); elemental analysis calcd (%) for $C_{24}H_{27}AlN_2O_2$: C 71.62, H 6.76, N 6.96; found: C 71.72, H 6.58, N 7.11.

Complex 3a: Obtained as a yellow solid in 96% yield. ^1H NMR (400 MHz, $CDCl_3$): δ = 7.77 (d, 4H, ArH), 7.24 (m, 6H, ArH), 5.79 (s, 2H, CHCOAl), 3.63 (b, 2H, $N(CH_2CH_2CH_2)N$), 3.41 (b, 2H, $N(CH_2CH_2CH_2)N$), 2.03 (s, 6H, CH_3CN), 1.91 (t, 2H, $N(CH_2CH_2CH_2)N$), 0.95 (t, 3H, $AlCH_2CH_3$), −0.06 ppm (q, 2H, $AlCH_2CH_3$); ^{13}C NMR (75 MHz, $CDCl_3$): δ = 173.0 (CH_3COAl), 172.3 (CH_3CN), 138.7, 129.7, 127.9, 126.9 (ArC), 97.1 (CHCOAl), 49.4 ($N(CH_2CH_2CH_2)N$), 26.2 ($N(CH_2CH_2CH_2)N$), 22.06 (CH_3CN), 10.4 ppm ($AlCH_2CH_3$); elemental analysis calcd (%) for $C_{25}H_{29}AlN_2O_2$: C 72.09, H 7.02, N 6.73; found C, 71.91, H 7.15, N 6.82.

Complex 4a: Obtained as a yellow solid in 98% yield. ^1H NMR (400 MHz, $CDCl_3$): δ = 7.93 (d, 4H, ArH), 7.36 (m, 6H, ArH), 5.84 (s, 2H, CHCOAl), 3.39 (s, 4H, $N(CH_2C(CH_3)_2CH_2)N$), 2.14 (s, 6H, CH_3CN), 1.09 (s, 3H, $N(CH_2C(CH_3)_2CH_2)N$), 0.97 (s, 3H, $N(CH_2C(CH_3)_2CH_2)N$), 0.85 (t, 3H, $AlCH_2CH_3$), −0.20 ppm (q, 2H, $AlCH_2CH_3$); ^{13}C NMR (75 MHz, $CDCl_3$): δ = 172.6, 171.8 (ArCOAl), 171.1, 170.2 (CH_3CN), 139.4, 129.9, 128.2, 126.2 (ArC), 97.5 (CHCOAl), 58.2 ($N(CH_2C(CH_3)_2CH_2)N$), 38.4 ($N(CH_2C(CH_3)_2CH_2)N$), 26.3 ($N(CH_2C(CH_3)_2CH_2)N$), 22.5 (CH_3CN), 10.4 ($AlCH_2CH_3$), −0.05 ppm ($AlCH_2CH_3$); elemental analysis calcd (%) for $C_{27}H_{33}AlN_2O_2$: C 72.95, H 7.48, N 6.30; found C, 72.63, H 7.85, N 6.05.

Complex 5a: Obtained as a yellow solid in 89% yield. ^1H NMR (400 MHz, $CDCl_3$): δ = 7.84 (d, 4H, ArH), 7.36 (m, 8H, ArH), 7.24 (d, 2H, ArH), 5.76 (s, 2H, CHCOAl), 4.64 (d, 4H, NCH_2ArCH_2N), 2.35 (s, 6H, CH_3CN), 0.91 (t, 3H, $AlCH_2CH_3$), −0.21 ppm (q, 2H, $AlCH_2CH_3$); ^{13}C NMR (100 MHz, $CDCl_3$): δ = 177.8 (ArCOH), 173.5 (CH_3CN), 138.3, 138.0, 129.5–124.9 (ArC), 98.0 (CHCOAl), 51.6 ($NCH_2C_6H_4CH_2N$), 22.6 (CH_3CN), 9.5 ($AlCH_2CH_3$), 0.2 ppm ($AlCH_2CH_3$); elemental analysis calcd (%) for $C_{30}H_{31}AlN_2O_2$: C 75.29, H 6.53, N 5.85; found C 75.40, H 6.88, N 6.13.

Complex 6a: Obtained as a yellow solid in 92% yield. ^1H NMR (300 MHz, $CDCl_3$): δ = 7.28 (m, 1H, ArH), 7.26 (m, 2H, ArH), 7.09 (m, 1H, ArH), 4.89 (s, 2H, CHCOAl), 4.48 (d, 4H, NCH_2ArCH_2N), 2.03 (s, 6H, CH_3COAl), 1.92 (s, 6H, CH_3CN), 0.90 (t, 3H, $AlCH_2CH_3$), −0.27 ppm (q, 2H, $AlCH_2CH_3$); ^{13}C NMR (100 MHz, $CDCl_3$): δ = 179.8 (CH_3COAl), 173.4 (CH_3CN), 140.0, 128.7, 125.3, 124.7 (ArC), 99.8 (CHCOAl), 52.4 ($NCH_2C_6H_4CH_2N$), 25.7 (CH_3COAl), 21.2 (CH_3CN), 9.35 ($AlCH_2CH_3$), −0.71 ppm ($AlCH_2CH_3$); elemental analysis calcd (%) for $C_{20}H_{27}AlN_2O_2$: C 67.78, H 7.68, N 7.90; found: C 68.07, H 7.44, N 7.52.

Complex 7a: Obtained as a yellow solid in 88% yield. ^1H NMR (400 MHz, $CDCl_3$): δ = 5.57 (s, 2H, CHCOAl), 3.64 (m, 2H, $N(CH_2CH_2)N$), 3.55 (m, 2H, $N(CH_2CH_2)N$), 2.14 (s, 6H, CH_3CN), 0.85 (t, 3H, $AlCH_2CH_3$), −0.34 ppm (q, 2H, $AlCH_2CH_3$); ^{13}C NMR (100 MHz, $CDCl_3$): δ = 161.7 (CF_3COH), 129.0 (CH_3CN), 119.4 (CF_3COH), 97.4 (CHCOH), 46.6 (NCH_2CH_2N), 21.8 (CH_3CN), 9.3 ($AlCH_2CH_3$), 1.0 ppm ($AlCH_2CH_3$); elemental analysis calcd (%) for $C_{14}H_{17}AlF_6N_2O_2$: C 43.53, H 4.44, N 7.25; found: C 43.63, H 4.21, N 7.65.

Complex 2b: Obtained as a yellow solid in quantitative yield. ^1H NMR (400 MHz, $CDCl_3$): δ = 7.34 (d, 4H, ArH), 7.17 (m, 6H, Ar*H*), 5.79 (s, 2H, C*H*COAl), 3.83 (sep, 1H, $OCH(CH_3)_2$), 3.69 (m, 2H, $N(CH_2CH_2)N$), 3.50 (m, 2H, $N(CH_2CH_2)N$), 2.05 (s, 6H, CH_3CN), 0.97 ppm (d, 6H, $OCH(CH_3)_2$); ^{13}C NMR (100 MHz, $CDCl_3$): δ = 173.3 (ArCOAl), 172.7 (CH_3CN), 138.6, 129.9, 128.1, 126.8 (ArC), 97.0 (CHCOAl), 62.7 ($OCH(CH_3)_2$), 46.4 (NCH_2), 27.5 ($OCH(CH_3)_2$), 22.5 ppm (CH_3CN); elemental analysis calcd (%) for $C_{25}H_{29}AlN_2O_3$: C 69.43, H 6.76, N 6.48; found: C 69.60; H,6.82, N 6.35.

Complex 4b: Obtained as a yellow solid in quantitative yield. ^1H NMR (400 MHz, $CDCl_3$): δ = 7.83 (m, 4H, Ar*H*), 7.29 (m, 6H, Ar*H*), 5.74 (s, 2H, C*H*COAl), 3.94 (m, 1H, $OCH(CH_3)_2$), 3.70 (d, 2H, $N(CH_2C(CH_3)_2CH_2)N$), 3.35 (d, 2H, $N(CH_2C(CH_3)_2CH_2)N$), 2.06 (s, 6H, CH_3CN), 1.04 (d, 6H, $OCH(CH_3)_2$), 1.00 (s, 3H, $N(CH_2C(CH_3)_2CH_2)N$), 0.88 ppm (s, 3H, $N(CH_2C(CH_3)_2CH_2)N$); ^{13}C NMR (100 MHz, $CDCl_3$): δ = 172.5 (ArCOAl), 172.1 (CH_3CN), 138.4, 129.8, 128.0, 126.9 (ArC), 97.4 (CHCOAl), 62.9 ($OCH(CH_3)_2$), 59.0 ($N(CH_2C(CH_3)_2CH_2)N$), 38.2 ($N(CH_2C(CH_3)_2CH_2)N$), 26.4 ($N(CH_2C(CH_3)_2CH_2)N$), 24.1 ($OCH(CH_3)_2$), 22.5 ppm (CH_3CN); elemental analysis calcd (%) for $C_{28}H_{35}AlN_2O_3$: C 70.86, H 7.43, N 5.90; found: C 70.59, H 7.12, N 5.75.

Polymerization of *rac*-LA Under the protection of argon, the *rac*-LA (22.4 mmol, 3.22 g), complexes **1a**–**7a**, (0.30 mmol in 2 mL of toluene), 2-propanol (0.30 mmol, in 5 mL of toluene), and toluene (38 mL) were added to a dried reaction vessel equipped with a magnetic stirring bar. The vessel was placed in an oil bath at 70°C. Conversion of the monomer was determined on the basis of ^1H NMR spectroscopic studies. The polymers were isolated by precipitation into cold methanol, then filtrated and dried under vacuum at RT for 24 h.

CCDC 659939, 659940, 659941, 659942, and 659943, contain the supplementary crystallographic data for this paper. These data can be obtained free of charge from The Cambridge Crystallographic Data Centre via www.ccdc.cam.ac.uk/data_request/cif.

Acknowledgements

This project is financially supported by the National Natural Science Foundation of China (Project No: 20574066), National Fund for Distinguished Young Scholar (No: 50425309), and the International Cooperation fund of Science and Technology (Key project 2005DFA50290).

[1] a) K. E. Uhrich, S. M. Cannizzaro, R. S. Langer, K. M. Shakesheff, *Chem. Rev.* **1999**, *99*, 3181; b) D. J. Mooney, G. Organ, J. P. Vacanti, R. Langer, *Cell Transplant.* **1994**, *2*, 203; c) J. L. Eguiburu, M. J. Fernandez-Berridi, F. P. Cossio, J. San Roman, *Macromolecules* **1999**, *32*, 8252.

[2] a) A.-C. Albertsson, I. K. Varma, *Biomacromolecules* **2003**, *4*, 1466; b) B. J. O'Keefe, M. A. Hillmyer, W. B. Tolman, *J. Chem. Soc. Dalton Trans.* **2001**, 2215; c) Z. Y. Zhong, P. J. Dijkstra, C. Birg, M. Westerhausen, J. Feijen, *Macromolecules* **2001**, *34*, 3863; d) D. Takeuchi, T. Nakamura, T. Aida, *Macromolecules* **2000**, *33*, 729; e) B. J. O'Keefe, L. E. Breyfogle, M. A. Hillmyer, W. B. Tolman, *J. Am. Chem. Soc.* **2002**, *124*, 4384.

[3] a) R. E. Drumright, P. R. Gruber, D. E. Henton, *Adv. Mater.* **2000**, *12*, 1841; b) E. Chiellini, R. Solaro, *Adv. Mater.* **1996**, *8*, 305.

[4] a) M. S. Reeve, S. P. McCarthy, M. J. Downey, R. A. Gross, *Macromolecules* **1994**, *27*, 825; b) J. R. Sarasua, ; R. E. Prud'homme, M. Wisniewski, A. Le Borgne, N. Spassky, *Macromolecules* **1998**, *31*, 3895; R. E. Prud'homme, M. Wisniewski, A. Le Borgne, N. Spassky, *Macromolecules* **1998**, *31*, 3895.

[5] a) M. Endo, T. Aida, S. Inoue, *Macromolecules* **1987**, *20*, 2982; b) A. Duda, Z. Florjanczyk, A. Hofman, S. Slomkowski, S. Penczek, *Macromolecules* **1990**, *23*, 1640; c) T. Aida, S. Inoue, *Acc. Chem. Res.* **1996**, *29*, 39; d) A. Kowalski, A. Duda, S. Penczek, *Macromol. Rapid Commun.* **1998**, *19*, 567; e) B. T. Ko, C. C. Lin, *Macromolecules* **1999**, *32*, 8296.

[6] a) A. Kowalski, A. Duda, S. Penczek, *Macromolecules* **2000**, *33*, 689; b) H. R. Kricheldorf, I. Kreiser-Saunders, A. Stricker, *Macromolecules* **2000**, *33*, 702.

[7] a) Y. Ikada, K. Jamshidi, H. Tsuji, S. H. Hyon, *Macromolecules* **1987**, *20*, 904; b) H. Tsuji, Y. Ikada, *Polymer* **1999**, *40*, 6699.

[8] N. Spassky, M. Wisniewski, C. Pluta, A. Le Borgne, *Macromol. Chem. Phys.* **1996**, *197*, 2627.
[9] a) T. M. Ovitt, G. W. Coates, *J. Am. Chem. Soc.* **2002**, *124*, 1316; b) C. P. Radano, G. L. Baker, M. R. Smith, *J. Am. Chem. Soc.* **2000**, *122*, 1552; c) Z. Y. Zhong, P. J. Dijkstra, J. Feijen, *Angew. Chem.* **2002**, *114*, 4692; *Angew. Chem. Int. Ed.* **2002**, *41*, 4510; d) Z. Y. Zhong, P. J. Dijkstra, J. Feijen, *J. Am. Chem. Soc.* **2003**, *125*, 11291; e) N. Nomura, R. Ishii, M. Akakura, K. Aoi, *J. Am. Chem. Soc.* **2002**, *124*, 5938; f) M. Wisniewski, A. LeBorgne, N. Spassky, *Macromol. Chem. Phys.* **1997**, *198*, 1227; g) Z. H. Tang, X. S. Chen, Y. K. Yang, X. Pang, J. R. Sun, X. F. Zhang, X. B. Jing, *J. Polym. Sci. Part A: Polym. Chem.* **2004**, *42*, 5974; h) Z. H. Tang, X. S. Chen, X. Pang, Y. K. Yang, X. F. Zhang, X. B. Jing, *Biomacromolecules* **2004**, *5*, 965; i) H. Y. Ma, G. Melillo, L. Oliva, T. P. Spaniol, U. Englert, J. Okuda, *Dalton. Trans.* **2005**, 721; j) K. Majerska, A. Duda, *J. Am. Chem. Soc.* **2004**, *126*, 1026; k) P. Hormnirun, E. L. Marshall, V. C. Gibson, A. J. P. White, D. J. Williams, *J. Am. Chem. Soc.* **2004**, *126*, 2688; l) R. Ishii, N. Nomura, T. Kondo, *Polym. J.* **2004**, *36*, 261.
[10] a) S. A. Schuetz, C. M. Silvernail, C. D. Incarvito, A. L. Rheingold, J. L. Clark, V. W. Day, J. A. Belot, *Inorg. Chem.* **2004**, *43*, 6203; b) S. A. Schuetz, V. W. Day, R. D. Sommer, A. L. Rheingold, J. A. Belot, *Inorg. Chem.* **2001**, *40*, 5292.
[11] X. Pang, H. Z. Du, X. S. Chen, X. L. Zhuang, D. M. Cui, X. B. Jing, *J. Polym. Sci. Part A: Polym. Chem.* **2005**, *43*, 6605.
[12] P. J. McCarthy, A. E. Martell, *Inorg. Chem.* **1967**, *6*, 781.
[13] a) D. A. Atwood, M. J. Harvey, *Chem. Rev.* **2001**, *101*, 37; b) M.-A. Munoz-Hernandez, T. S. Keizer, P. Wei, S. Parkin, D. A. Atwood, *Inorg. Chem.* **2001**, *40*, 6782.
[14] H. Y. Chen, H. Y. Tang, C. C. Lin, *Macromolecules* **2006**, *39*, 3745.
[15] R. Benn, A. Rufinska, H. Lemkuhl, E. Janssen, C. Kruger, *Angew. Chem.* **1983**, *95*, 808; *Angew. Chem. Int. Ed. Engl.* **1983**, *22*, 779.
[16] J. Baran, A. Duda, A. Kowalski, R. Szymanski, S. Penczek, *Macromol. Rapid Commun.* **1997**, *18*, 325.
[17] Kinetic studies of **2a** and **3a** have been reported, see ref. [11].
[18] a) H. R. Kricheldorf, S. R. Lee, S. Bush, *Macromolecules* **1996**, *29*, 1375; b) W. M. Stevels, P. J. Dijkstra, J. Feijen, *Trends Polym. Sci.* **1997**, *5*, 300; c) P. Dubois, C. Jacobs, R. Jerome, P. Teyssie, *Macromolecules* **1991**, *24*, 2266; d) A. Kowalski, A. Duda, S. Penczek, *Macromolecules* **1998**, *31*, 2114; e) A. Kowalski, A. Duda, S. Penczek, *Macromolecules* **2000**, *33*, 689.
[19] A. Amgoune, C. M. Thomas, T. Roisnel, J.-F. Carpentier, *Chem. Eur. J.* **2006**, *12*, 169.
[20] B. M. Chamberlain, M. Cheng, D. R. Moore, T. M. Ovitt, E. B. Lobkovsky, G. W. Coates, *J. Am. Chem. Soc.* **2001**, *123*, 3229.
[21] P_m is the probability of *meso* linkages, according to $[mmm]=P_m^2+(1-P_m)P_m/2$, $[mmr]=[rmm]=(1-P_m)P_m/2$, $[rmr]=(1-P_m)^2/2$, $[mrm]=[(1-P_m)^2+P_m(1-P_m)]/2$.
[22] D. R. Witzke, R. Narayan, J. J. Kolstad, *Macromolecules* **1997**, *30*, 7075.
[23] 3a and 4a had same τ value and almost same Pm value; 2a contained lower τ value (0.09) and had lower P_m (see Table 2). Further evidence came from the τ values of real initiators **2b** (τ value 0.54) and **4b** (τ value 0.85) and the P_m values of **2b** (P_m value 0.69) and **4b** (P_m value 0.78).
[24] a) K. A. M. Thakur, R. T. Kean, E. S. Hall, J. J. Kolstad, E. J. Munson, *Macromolecules* **1998**, *31*, 1487; b) K. A. M. Thakur, R. T. Kean, M. T. Zell, B. E. Padden, E. J. Munson, *Chem. Commun.* **1998**, *17*, 1913; c) M. H. Chisholm, S. S. Iyer, M. E. Matison, D. G. McCollum, M. Pagel, *Chem. Commun.* **1997**, *20*, 1999.
[25] a) M. Wisniewski, A. LeBorgne, N. Spassky, *Macromol. Chem. Phys.* **1997**, *198*, 1227; b) J. E. Kasperczyk, *Macromolecules* **1996**, *29*, 3937.
[26] P. J. Hocking, R. H. Marchessault, *Macromolecules* **1995**, *28*, 6401.

Received: September 17, 2007
Published online: January 29, 2008

